

See discussions, stats, and author profiles for this publication at: <https://www.researchgate.net/publication/270650071>

# Effects of Momentum Ratio and Weber Number on Spray Half Angles of Liquid Controlled Pintle Injector

Article in *Journal of Thermal Science* · February 2015

DOI: 10.1007/s11630-015-0753-7

---

CITATIONS  
27

READS  
2,586

---

5 authors, including:



Min Son

Universität der Bundeswehr München

64 PUBLICATIONS 201 CITATIONS

[SEE PROFILE](#)



Jaye Koo

Korea Aviation University

139 PUBLICATIONS 494 CITATIONS

[SEE PROFILE](#)

Some of the authors of this publication are also working on these related projects:



Development of Module Program for Combustor/Gas generator/Starter in Liquid Rocket Engine [View project](#)



Fundamentals of modern technologies for thrust generators relevant to propulsion applications: Experimental study on pulse detonation engines [View project](#)

## Effects of Momentum Ratio and Weber Number on Spray Half Angles of Liquid Controlled Pintle Injector

Min Son<sup>1</sup>, Kijeong Yu<sup>1</sup>, Jaye Koo<sup>2</sup>, Oh Chae Kwon<sup>3</sup>, Jeong Soo Kim<sup>4</sup>

1. Graduate Student, Korea Aerospace University, Goyang, Republic of Korea

2. School of Aerospace and Mechanical Engineering, Korea Aerospace University, Goyang, Republic of Korea

3. School of Mechanical Engineering, Sungkyunkwan University, Suwon, Republic of Korea

4. Department of Mechanical Engineering, Pukyong National University, Busan, Republic of Korea

© Science Press and Institute of Engineering Thermophysics, CAS and Springer-Verlag Berlin Heidelberg 2015

A pintle injector is advantageous for throttling a liquid rocket engine and reducing engine weight. This study explores the effects of momentum ratio and Weber number at various injection conditions on spray characteristics of the pintle injector for liquid-gas propellants. A liquid sheet is injected from a center pintle nozzle and it is broken by a gas jet from an annular gap. The pressure drops of propellants, and the pintle opening distance were considered as control variables; using 0.1 ~ 1.0 as a bar for the pressure drop of the liquid injection, a 0.01~0.2 bar for the pressure drop of gas jet and a 0.2 ~ 1.0 mm for the pintle opening distance. The discharge coefficient was decreased linearly before the pintle opening distance of 0.75 mm and then, the coefficient was slightly increased. Spray images were captured by a CMOS camera with high resolution. Then, the shadow and reflected images were analyzed. Spray distributions were measured by a patternator with an axial distance of 50 mm from a pintle tip. Finally, the spray half angles had an exponentially decreasing correlation as a momentum ratio divided by the Weber number. Also, the spray half angles from the spray distribution were underestimated compared to those measured from the captured images.

**Keywords:** Pintle Injector, Spray Half Angle, Spray Distribution, Visualization

### Introduction

In order to develop a liquid rocket engine with low cost and throttle ability, a pintle injector was selected as the best choice for the injection system. The pintle injector is able to control the mass flow rate of propellants and its spray characteristics allow for a single injector system. The original pintle injector was developed from an experimental device used to study reaction rates of hypergolic propellants in the 1950s [1]. The pintle injector was

mainly developed as the rocket injector for TRW Inc. and was used for a lunar exploration module in 1969 [2,3]. Currently, the pintle injector is being used by Space X and Northrop Grumman Aerospace Systems to develop a low-cost engine [4,5]. Fundamental research of the pintle is mainly led by a group from Purdue University using a new type of injector, the face shut-off type [6,7]. Because the pintle injector has a more complex structure than other rocket injectors, such as the shear coaxial injector or the swirl injector, it is difficult to reveal the spray cha-

---

Received: September 2014      Jaye Koo: Professor

This work was supported by Advanced Research Center Program (NRF-2013R1A5A1073861) through the National Research Foundation of Korea(NRF) grant funded by the Korea government(MSIP) contracted through Advanced Space Propulsion Research Center at Seoul National University.

[www.springerlink.com](http://www.springerlink.com)

<b>Nomenclature</b>		$\sigma$	surface tension (N/m)
		<b>Subscripts</b>	
$A$	area ( $m^2$ )	$cg$	center gap
$C_d$	discharge coefficient	$cp$	center post
$D$	diameter (mm)	$gas$	gaseous
$H$	height (mm)	$ib$	inner body
$L$	distance (mm)	$liq$	liquid
$\dot{m}$	mass flow rate ( $kg/s$ )	$M$	measured
$M$	momentum ratio	$ob$	outer body
$\Delta P$	injection pressure drop (bar)	$pe$	pintle end
$t$	thickness (mm)	$pg$	pintle gap
$V$	velocity (m/s)	$pr$	pintle rod
We	Weber number	$pt$	pintle tip
<b>Greek letters</b>		$Tot$	total
$\alpha$	spray half angle	$w$	water
$\rho$	density ( $kg/m^3$ )		

racteristics of the pintle injector.

Also, new concepts should be developed to overcome the critical disadvantage of the pintle injector, such as its thermal vulnerability of the protruded pintle tip. In this study, spray characteristics were analyzed using a traditional pintle injector with a moving pintle. In order to target liquid oxygen and gaseous methane, a combination of liquid and gas was selected.

## Experimental Apparatus and Conditions

### Pintle injector and experimental conditions

A simple type of movable pintle was used as shown in Fig. 1. An oxidizer is injected from a center nozzle which is the pintle post and distributed along the surface of the pintle tip. Fuel is injected axially from an annular gap and impinges on the oxidizer sheet. The pintle can be controlled on an axial direction by using a micrometer with resolution of a unit micron. In this case, the pintle

tip was designed larger than a pintle post. The major dimensions of the injector are listed in Table 1. The distance of the pintle gap was an important shape variable.

Because we targeted liquid oxygen and methane as propellants, water and air were used as simulants of the propellants to study breakup characteristics in standard conditions. Pressure drops of injector gaps in working condition were restricted as shown in Table 1. The pintle gap was also controlled from 0.2 mm to 1.0 mm.

**Table 1** Dimensions of the pintle injector and experimental conditions

Dimensions		
Outer body diameter	$D_{ob}$	13.5 mm
Inner body diameter	$D_{ib}$	12.0 mm
Center gap diameter	$D_{cg}$	4.0 mm
Center post diameter	$D_{cp}$	8.0 mm
Pintle rod diameter	$D_{pr}$	3.0 mm
Pintle tip diameter	$D_{pt}$	12.0 mm
Center post length	$L_{pt}$	5.0 mm
Pintle tip thickness	$t_{pt}$	3.0 mm
Pintle end thickness	$t_{pe}$	1.0 mm
Pintle opening distance	$L_{open}$	0.2 ~ 1.0 mm
Experimental conditions		
Pressure drop in pintle gap (liquid)		0.1 ~ 1.0 barg
Pressure drop in annular gap (gas)		0.01 ~ 0.2 barg

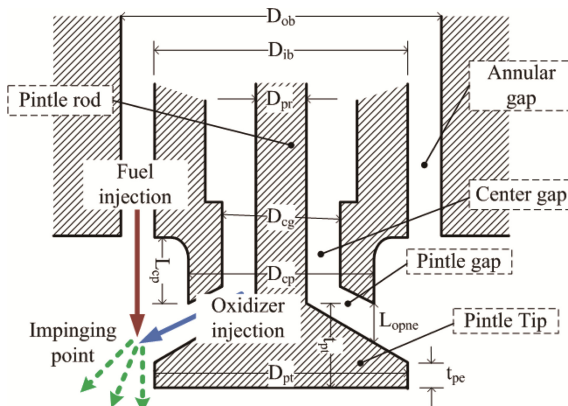


**Fig. 1** Schematic of pintle injector

### Recirculating supply system

In order to continuously supply water as the simulant of the oxidizer, a recirculating supply system was used as

shown in Fig. 2. Water was pressurized by a piston pump and a reservoir was used as a pre-accumulator. The supply pressure of water was controlled by a metering valve and two bypass valves. Injected water was collected in a cistern and was processed through a strainer before recycled back through the system. Air was supplied separately from a tank pressurized by a compressor.

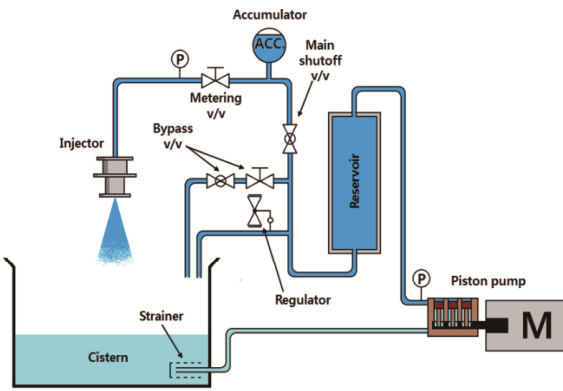


**Fig. 2** Experiment apparatus for recirculating water supply

### Measurement system

Two methods were applied to analyze the spray characteristics. One is image capturing and the other is spray patterning. Figure 3 presents a visualization method to capture instant images and averaged images using a CMOS camera with high resolution. While the instant snapshots were captured from the camera which was arranged in a straight line with a strobe scope, the camera for the averaged images was arranged at 45 degrees. From the spray images, breakup features and spray half angles were analyzed at various conditions.

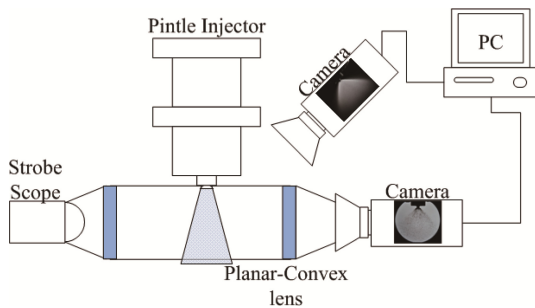


**Fig. 3** Visualization system to capture spray images

In order to compare spray distributions, a patterner was adopted as shown in Fig. 4. The patterner consisted of 49 cylinders aligned in a seven-by-seven mesh. The injected and broken droplets were accumulated and the water height in each cylinder was measured by an ultrasonic sensor for non-contact distance measurement. Measured heights of the water were converted to normalized mass distribution.

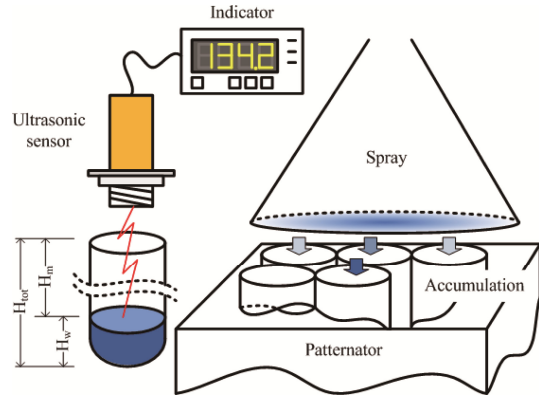


**Fig. 4** Patterner and measurement system

## Results and discussion

### Discharge coefficients

The pintle injector has variable nozzle diameters at different opening distances, thus, the minimum area of mass flow rate is determined. There are some significant major gaps near the pintle nozzle as shown in Fig. 5.  $L_{cg}$  is the distance of the gap near the center and  $L_{open}$  is the distance from the center post to the pintle in an axial direction. However, the most important gap is  $L_{pg}$  because it regulates the minimum area. As the pintle moves from the zero opening distance, the mass flow rate increases as shown in Fig. 6. At some point the  $L_{pg}$  is the same as  $L_{cg}$ , and the minimum gap is changed to the center gap. Accordingly, if the center gap is constant, the mass flow rate is theoretically constant.

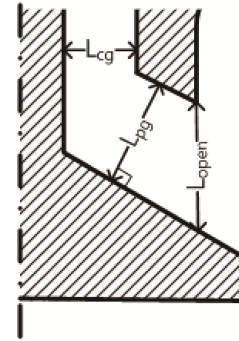


**Fig. 5** Major gaps near pintle nozzle

In contrast, the actual mass flow rates were different to the theoretical assumption as shown in Fig. 7. After the theoretical point of area changed, the mass flow rate still increased. It seems that there were recirculation zones near the center post corner. As a result, the actual orifice size of the pintle gap could be smaller than the estimated one and the orifice size could change due to the opening distance. The discharge coefficients,  $C_d$ , at various conditions were derived from Eq. (1) and the results are shown in Fig. 8. Up to the opening distance of about 0.75 mm,

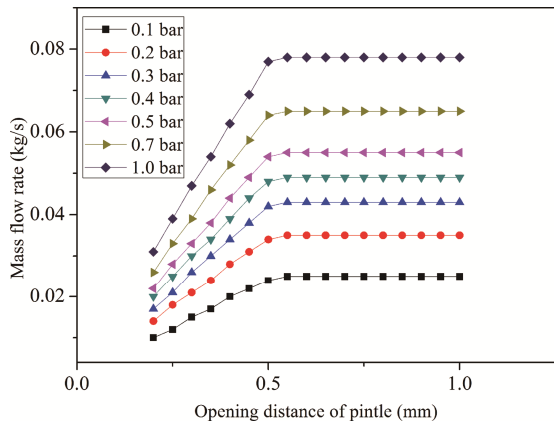


**Fig. 6** Theoretical mass flow rates of water with various water pressure drops and pindle opening distances

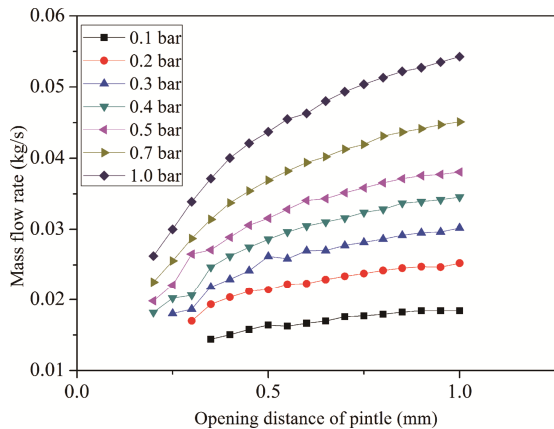


**Fig. 7** Actual mass flow rates of water with various water pressure drops and pindle opening distances

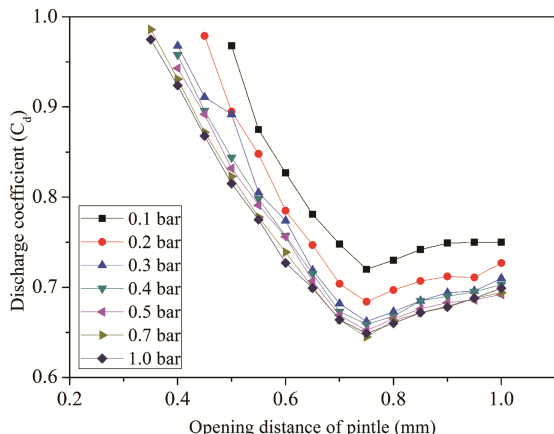


**Fig. 8** Discharge coefficients with various water pressure drops and pindle opening distances

the discharge coefficients decreased linearly and then increased slightly after about 0.75 mm. At the same opening distance, the discharge coefficients were higher for lower pressure drop.

$$C_d = \frac{\dot{m}_{liq}}{A_{liq} \sqrt{2\rho_{liq} \Delta P_{liq}}} \quad (1)$$

### Spray images

Fig. 9 shows the spray images from the shadow method. The images were taken at opening distances from 0.2 ~ 0.8 mm, liquid pressure drops from 0.1 ~ 1.0 bars and gas pressure drops of 0.01 ~ 0.20 bars. At low pressure drops of liquid, a very narrow liquid sheet was constructed by low liquid momentum. In most cases, higher gas pressure drops resulted in higher breakup performance and the droplets were very fine after the gas pressure drop of 0.2 bars. The detailed breakup characteristics will be conducted in future work.

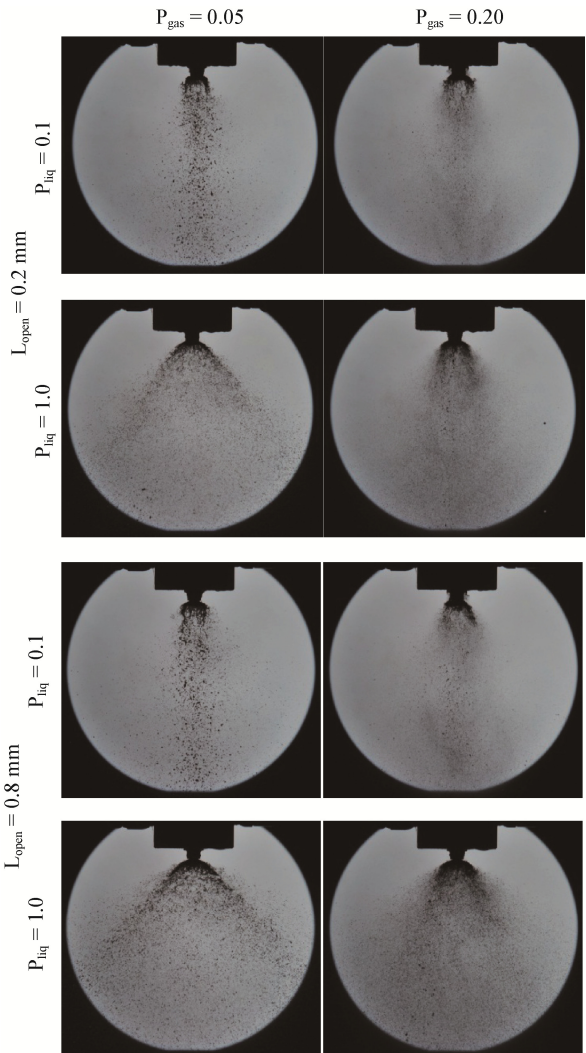


**Fig. 9** Shadowgraph spray images at various conditions

In order to measure the spray half angle in detail, the images were captured with long exposure time by a camera arranged diagonally at 45 degrees. In addition, post-

processing for the images was performed to clarify the spray boundaries. Fig. 10 presents a flowchart of the post-process. Finally the converted images were sorted as shown in Fig. 11. The spray half angle was measured using spray widths at an axial distance of 50mm away from the pintle tip as shown in Fig. 12. The spray half angles largely increased when liquid pressure drop was 0.1 bar and the spray half angles converged to an upper limit for all cases as shown in Fig. 13.

Two non-dimensional parameters were selected to derive correlations with the spray half angle; Momentum ratios and Weber numbers. The parameters for all experimental cases were distributed as shown in Fig. 14 and

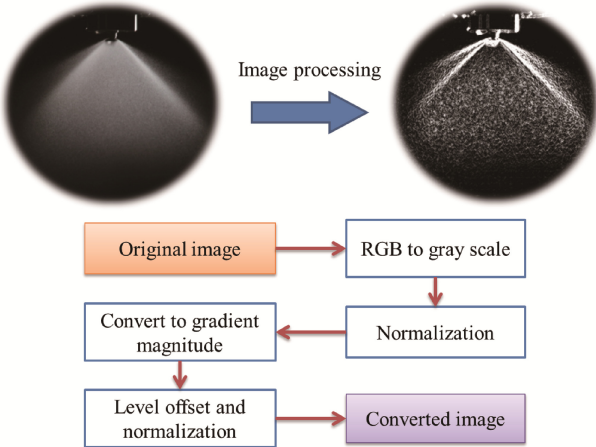


**Fig. 10** Flow chart of image processing method

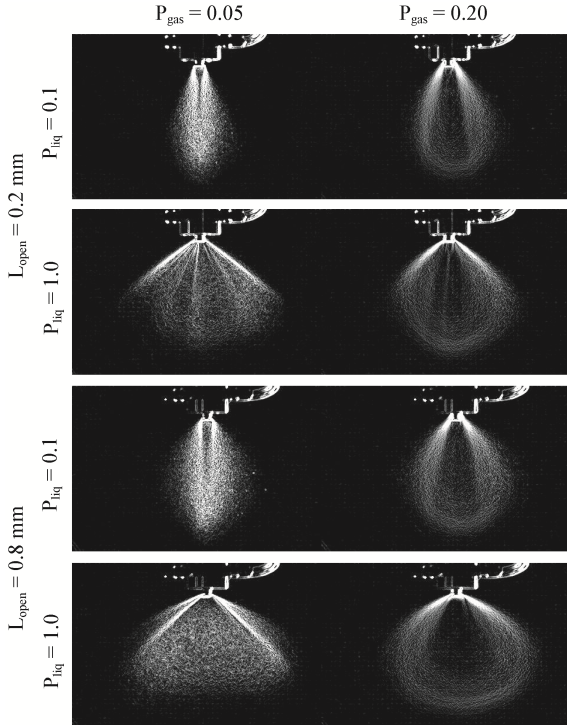


**Fig. 11** Converted spray images at various conditions

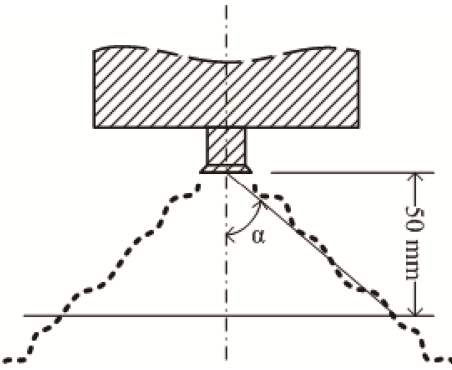


**Fig. 12** Definition of spray half angle

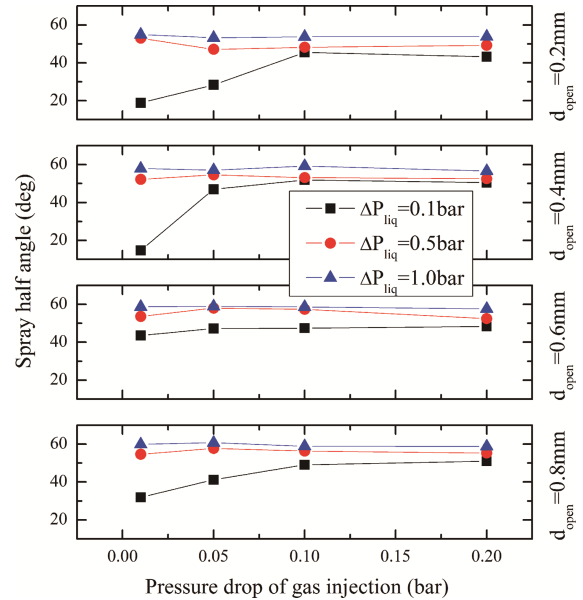


**Fig. 13** Spray half angles from captured images with various experimental conditions.

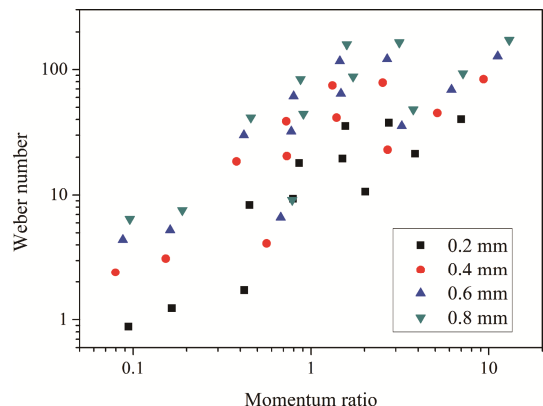


**Fig. 14** Momentum ratios and weber numbers in experimental conditions with various pintle opening distances

the parameters were calculated using Eq. (2) and (3) with the measured mass flow rates and pressure drops.

$$M = \frac{\dot{m}_{\text{gas}} V_{\text{gas}}}{\dot{m}_{\text{liq}} V_{\text{liq}}} \quad (2)$$

$$We = \frac{\rho_{\text{gas}} (V_{\text{gas}} - V_{\text{liq}})^2 d_{\text{open}}}{\sigma_{\text{liq}}} \quad (3)$$

With the non-dimensional parameters, there is a specific correlation as shown in Fig. 15. From the regression method, the spray half angle follows the trend as expressed in Eq. (4).

$$\alpha = 38.86 \left( \frac{M}{We} \right)^{-0.096} \quad (4)$$

At the region of lower spray half angles, the liquid sheet was not perfectly formed and that caused too much low spray half angles for some cases. So there was a transition interval at the low opening distance and the low liquid pressure drop. Therefore, this transition phenomenon should be studied independently in future work for a low thrust control of a rocket engine.

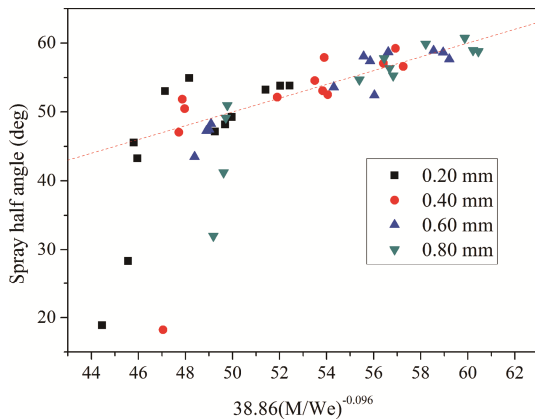


Fig. 15 Comparison of spray half angles and correlation

### Spray pattern and distribution

For the rocket application, mixing characteristics are also important design points. As an estimation method for mixing performance, patterns of spray cross section were measured by the patternator and the result is summarized in Fig. 16. At a low pressure drop of liquid of 0.1 bars, the cross section of spray increased as the gas assist enhanced. However, the spray area decreased as the gas pressure drop decreased at the higher injection pressure of liquid. Additionally, the spray became concentrated in the center as the gas jet enhanced and as the opening distance decreased.

The spray half angles could also be measured from the spray distributions as shown in Fig. 17. Only for the liquid pressure drop of 0.1 bars, the spray half angle increased as the gas pressure drop increased and the spray half angle decreased at a higher pressure drop of liquid. As with the spray half angle result from the spray images, there is a similar trend shown in Fig. 18. It was different

in that the result from the spray patterns was more dispersed than that from the spray images. Consequently, the spray half angle had a correlation as expressed in Eq. (5) and it was underestimated.

$$\alpha = 28.67 \left( \frac{M}{We} \right)^{-0.124} \quad (5)$$

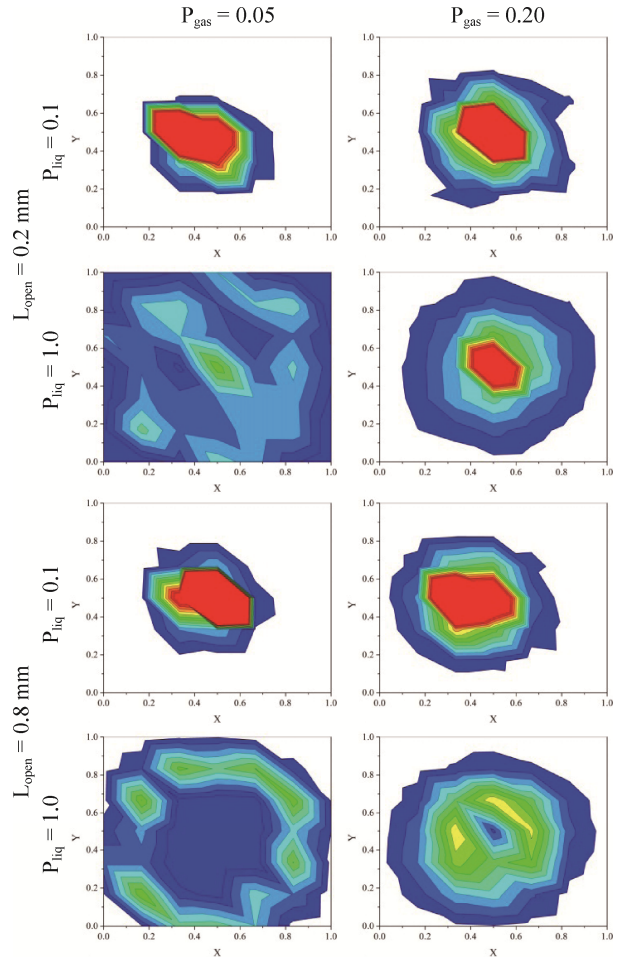
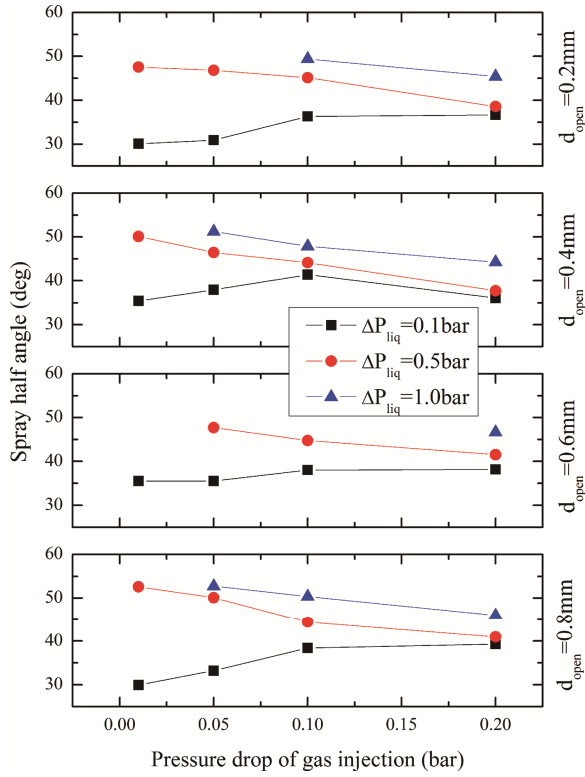


Fig. 16 Spray distributions at various conditions

### Conclusions

In this study, spray characteristics were studied from a liquid sheet which was injected from a pintle nozzle and broken by a gas jet from an annular gap. Mass flow rates and discharge coefficients were estimated based on various opening distances of pintle and injection pressures. The discharge coefficient was decreased linearly before the pintle opening distance of 0.75 mm and then, the coefficient slightly increased. Spray images were captured in two different ways and spray distributions were measured by a patternator. As a result, the spray half angle had correlation with the momentum ratio and Weber number in all experimental conditions except the lower pressure drop of liquid injection.



**Fig. 17** Spray half angles from spray patterns with various experimental conditions.

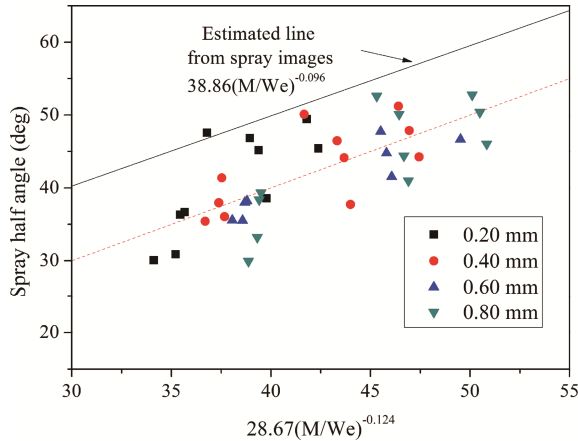


**Fig. 18** Comparison of spray half angles from patterns and correlation

## Acknowledgement

This work was supported by Advanced Research Center Program (NRF-2013R1A5A1073861) through the National Research Foundation of Korea(NRF) grant funded by the Korea government(MSIP) contracted through Advanced Space Propulsion Research Center at Seoul National University.

## References

- [1] G. A. Dressler and J. M. Bauer, TRW Pintle Engine Heritage and Performance Characteristics, 36th AIAA/ ASME/SAE/ASEE Joint Propulsion Conference and Exhibit, Huntsville, AL, 2000.
- [2] R. Gilroy and R. Sackheim, The Lunar Module Descent engine-A Historical Summary, 25th AIAA/ ASME/ SAE/ ASEE Joint Propulsion Conference and Exhibit, Monterey, CA, 1989.
- [3] M. J. Casiano, J. R. Hulk, and V. Yang, Liquid-Propellant Rocket Engine Throttling: A Comprehensive Review, Journal of Propulsion and Power, Vol. 26, No. 5, 2010.
- [4] J. Calvignac, L. Dang, T. L. Tramel, and L. Paseur, Design and Testing of Non-Toxic RCS Thrusters For Second Generation Reusable Launch Vehicle, 39th AIAA/ASME/ SAE/ASEE Joint Propulsion Conference and Exhibit, Huntsville, AL, 2003.
- [5] J. M. Gromski, A. N. Majamaki, S. G. Chianese, V. D. Weinstock and T. S. Kim, Northrop Grumman TR202 LOX/LH<sub>2</sub> Deep Throttling Engine Technology Project Status, 46th AIAA/ASME/SAE/ASEE Joint Propulsion Conference & Exhibit, Nashville, TN, 2010.
- [6] M. J. Bedard, T. W. Feldman, A. Rettenmaier, and W. Anderson, Student Design/Build/Test of a Throttleable LOX-LCH<sub>4</sub> Thrust Chamber, 48th AIAA/ASME/SAE/ ASEE Joint Propulsion Conference & Exhibit, Atlanta, GA, 2012.
- [7] B. L. Austin, S. D. Heister, and W. E. Anderson, Characterization of Pintle Engine Performance for Nontoxic Hypergolic Bipropellants, Journal of Propulsion and Power, Vol. 21, No. 4, 2005.